Phase Structures, Transition Behavior, and Surface Alignment in Polymers Containing Rigid-Rod Backbones with Flexible Side Chains. 4. Solid-State ^{13}C NMR Studies of Molecular Motions in PEFBPs(*n*) (*n* = 10 and 11)

Jason J. Ge, Mingming Guo,* Zhanhui Zhang, Paul S. Honigfort, Ian K. Mann, Shyh-Yeu Wang, Frank W. Harris, and Stephen Z. D. Cheng*

Maurice Morton Institute and Department of Polymer Science, The University of Akron, Akron, Ohio 44325-3909

Received December 22, 1998; Revised Manuscript Received March 2, 2000

ABSTRACT: "Combined" main-chain/side-chain liquid crystalline (LC) polyesters have been investigated using carbon-13 nuclear magnetic resonance (^{13}C NMR), based on the polycondensation of 2,2′-bis-(trifluoromethyl)-4,4′-biphenyldicarbonyl chloride with 2,2′-bis{*ω*-[4-(4-cyanophenyl)phenyoxy]-*n*-alkoxy-carbonyl]}-4,4′-biphenyl diol, abbreviated as PEFBP(*n*). Variable-temperature cross polarization/magic angle spinning and Bloch decay techniques have been applied to detect the rigid and mobile components of the different ordered structures of PEFBPs(*n*) (*n* = 10 and 11). Upon heating, PEFBP(10) possesses a smectic A (S_A) phase at low temperatures followed by a nematic (N) phase, and finally, the isotropization. PEFBP(11) exhibits a low-temperature crystalline (K_O) phase, two high-temperature crystalline (K_{T1} and K_{T2}) phases, and a N phase prior to isotropization. The NMR analyses indicate that the backbones and side-chain mesogens are involved in both the formation of the N phases and the construction of the smectic and crystalline structures. The detectable gauche conformations of the methylene units in the side chains provide experimental evidence that both the side-chain mesogens and the backbones parallel align and pack into one crystal lattice or LC phases. The proton spin−lattice relaxation in the rotating frame ($^{H}T_{1\rho}$) and spin−spin relaxation ($^{H}T_2$) experiments show single-exponential decays of intensities with respect to the spin lock time or delay time in both the S_A phase of PEFBP(10) and the crystalline phases of PEFBP(11), indicating that the systems have uniform dynamics. The side chains and the backbones are not separated into individual domains on a scale of several nanometers in the S_A phase of PEFBP(10) and the crystalline K_{T2} phase of PEFBP(11).

Introduction

Recently, considerable attention in the field of liquid crystalline polymers (LCPs) has been emphasized on the design of a variety of LCP architectures containing bulky pendant mesogens. The incorporation of bulky pendant mesogens can result in specific linear or nonlinear optical properties, which are useful in optical devices.[1−3] For example, the discovery of *p*-cyanobiphenyl-based LC molecules lead to the first commercial liquid crystal displays.[4] Moreover, "combined" main-chain/side-chain LCPs have also been synthesized via the direct attachment of mesogens along the chain backbone as well as along the side chains.[5−9] The presence of mesogens in both the backbones and side chains may lead to intriguing structural organizations as well as potential optical applications.

A series of "combined" LC polyesters [PEFBP(*n*)] containing pendant 4-cyanobiphenyl mesogens has been synthesized by the polycondensation of 2,2′-bis(trifluoromethyl)-4,4′-biphenyldicarbonyl chloride with 2,2′-bis{*ω*-[4-(4-cyanophenyl)phenyoxy]-*n*-alkoxycarbonyl]}-4,4′-biphenyl diol.[10] The phase structures, phase transition kinetics, morphologies, and the odd−even effect of the phase transition behavior have been previously reported.[11−13] These polymers may also be viewed as modified hairy-rod polymers with pendent mesogens attached to paraffin side chains. In hairy-rod polymers, a sanidic (board-like) structural model was proposed based on the microphase separation wherein the two-dimensional backbones stack together to form rigid-rod molecular sheets sandwiched by layers of paraffin side chains.[14−17] In these sanidic structures, the low-temperature transition is associated with the disordering of the side chains and above this temperature the rigid-rod backbones must be immersed in a medium of molten side chains. The high-temperature transition is associated with the isotropization of the backbones.

It has been reported that PEFBPs with even-numbered methylene (CH_2) units exhibit different phase behavior compared to those with odd-numbered CH_2 units.[11−13] For example, PEFBPs(*n* = 8 and 10) possess a low-temperature smectic (S_A) phase, which transforms into a nematic (N) phase at a certain temperature before entering the isotropic (I) state. However, the phase transitions of PEFBPs(*n*) (*n* = 9 and 11) involve the formation of crystalline structures, leading to phase transition sequences critically dependent upon the heating rate. Two triclinic (K_T) phases have been observed in PEFBP(11) in addition to a low-temperature orthorhombic (K_O) phase. One K_O phase and one K_T phase have been identified in PEFBP(9). The K_T phases of these systems have high crystallinity with unusually large lateral unit cell (*a*- and *b*-axes) dimensions. The lateral unit cell dimensions of the crystals in PEFBP(9) are smaller than those in PEFBP(11), but their c-axes

* To whom correspondence should be addressed. E-mail: cheng@polymer.uakron.edu.

10.1021/ma981970y CCC: $19.00
Published on Web 04/27/2000

along the backbones are almost identical. This indicates that the lateral dimensions in the crystalline lattice are associated with the arrangement of the aliphatic side chains, implying that the main-chain backbones and the side-chain mesogens are cooperatively packed in the crystalline phases.

Solid-state carbon-13 nuclear magnetic resonance (^{13}C NMR) is a useful technique for probing the changes in the electron environment of ^{13}C nuclei in the condensed state.[18−22] Variable-temperature cross-polarization (CP), measured under magic angle spinning (MAS) along with dipolar decoupling (DD) can distinguish between carbon nuclei with different electron environments (related to conformations) of the rigid components. This is based upon characteristic chemical shifts and spin populations (signal intensities) of distinguishable resonances. Bloch decay is another powerful tool for detecting mobile components. In addition, proton spin−spin and spin−lattice relaxation processes are used to determine proton relaxation times ($^{H}T_2$ and $^{H}T_{1\rho}$) in identifying if the system is homogeneous or heterogeneous in terms of proton spin diffusions. In this study, we report our solid-state ^{13}C NMR experimental results of PEFBPs(*n*) (*n* = 10 and 11) from the viewpoint of molecular motions.

Experimental Section

Materials and Samples. The synthesis of this series of combined LC polyesters was previously reported.[10,11] The intrinsic viscosities for PEFBPs(*n*) (*n* = 10 and 11) are 0.36 and 0.40 dL/g in chloroform at 30 °C, respectively. The samples were cooled at a rate of 1 °C/min from the isotropization temperature to room temperature. NMR measurements can thus be carried out in all crystalline and LC phases upon heating.

Equipment and Experiments. Solid-state ^{13}C NMR experiments were conducted on a Chemagnetics CMX 200 spectrometer operating at 201.13 and 50.78 Hz for ^{1}H and ^{13}C nuclei, respectively. The solid-state probe of this instrument (a Zr_2O_3 sample rotor with a diameter of 7.5 mm) had a wide temperature range of −100 to +200 °C. The samples were spun in nitrogen gas at 4.5 kHz at the magic angle.

The ^{13}C CP/MAS/DD NMR spectra were acquired over a temperature region above the T_g in order to selectively investigate the rigid components in these polymers. The proton decoupling field was of the same strength as the spin-lock field. The magic angle was optimized by the intensity calibration of the aromatic carbon resonance of hexamethylbenzene. The contact time was 1 ms. The Bloch decay spectra with MAS were conducted to selectively study the mobile components. To match the corresponding analyses of differential scanning calorimetry (DSC) and wide-angle X-ray diffraction (WAXD) measurements reported earlier,[11−13] the ^{13}C NMR spectra were recorded in an isothermal state after a preset temperature was reached at a heating rate of 1 °C/min and held isothermally for 30 min. Each spectrum consists of an accumulation of 300 scans for PEFBP(11), and 600 scans for PEFBP(10). The proton 90°−pulse width was set at 4.3 μs for ^{13}C, and the recycle delay between the successive pulse sequences was 5 s. Gated high-power proton decoupling at 63 kHz was used to avoid the nuclear Overhauser effect.

The proton spin−lattice relaxation time in the rotating frame ($^{H}T_{1\rho}$) was measured based on the intensity change in the ^{13}C CP/MAS spectra as a function of the proton spin lock time (0.01−40 ms). The pulse sequence was ^{1}H(90°x)(τy) followed by simultaneous 1 ms ^{13}C and ^{1}H spin locks, which was followed by acquisition of the ^{13}C magnetization with proton dipolar coupling. The proton 90°-pulse length was 4 μs at a spin rate of 4.5 kHz, with a contact time of 1 ms and a recycle time of 4 s. The proton spin lock field was employed at 62.5 kHz, matching the spin lock polarization transfer. The CP/MAS proton spin−spin relaxation time $^{H}T_2$ was measured as the intensity changed in the ^{13}C CP/MAS spectra as a function of the delay time (1−60 μs) between the proton 90°-pulse and cross polarization.[23]

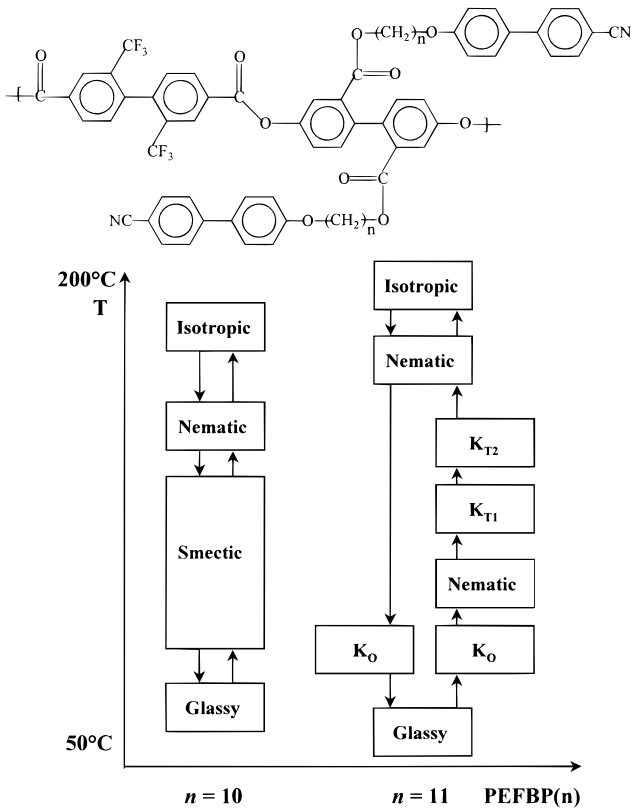

Figure 1. Schematic representation of the phase transition sequences for PEFBPs(*n*) (*n* = 10 and 11) during both cooling and subsequent heating at 1 °C/min.

Results and Discussion

Summary of the Phase Structures and Transition Behaviors in PEFBPs(*n*) (*n* = 10 and 11). Identification of the phase structures and transitions in these two PEFBPs(*n*) (*n* = 10 and 11) was achieved using the combined experimental techniques of DSC, WAXD, polarized light microscopy, transmission electron microscopy, and electron diffraction.[11−13] Figure 1 illustrates the phases and phase transition sequences of PEFBPs(*n*) (*n* = 10 and 11) at cooling and heating rates of 1 °C/min. In PEFBP(10), neither the N nor S_A phases can be bypassed during cooling or heating. The S_A phase is observed above the T_g of 63 °C (the S_A LC glass). The $S_A \rightarrow$ N transition occurs at 170 °C. The N $\rightarrow$ I transition occurs at 177 °C. This two-phase transition sequence is reversible upon cooling.[13]

PEFBP(11) exhibits a more complicated crystalline and LC phase transition behavior. Upon cooling, in addition to the high-temperature N phase, a low-temperature orthorhombic K_O crystal phase is observed. However, other phase transitions can be formed upon heating at 1 °C/min. Above its T_g of 50 °C, the sample enters the K_O phase which melts at 100 °C into the N phase. Upon further heating, the polymer recrystallizes to form two triclinic crystalline (K_{T1} and K_{T2}) phases, entering the N phase at 170 °C. Finally, isotropization is reached at 193 °C.[11]

Chemical Shifts of PEFBPs(*n*) (*n* = 10 and 11). To identify the chemical shifts of the ^{13}C nuclei of the side chains of PEFBPs(*n*) (*n* = 10 and 11) in NMR

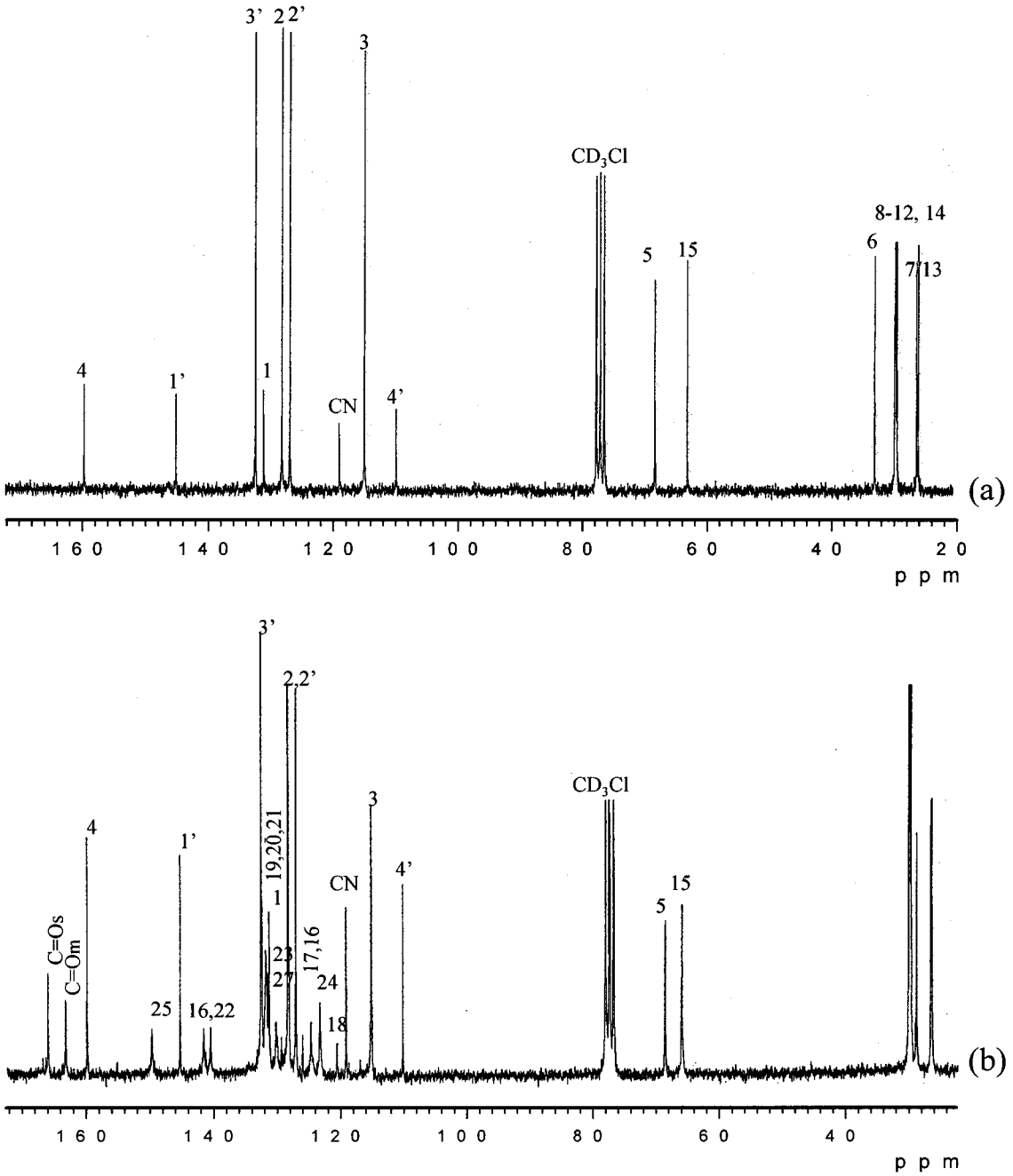

Figure 2. Solution ^{13}C NMR spectra of (a) the 11-OCB LC model component and (b) PEFBP(11).

spectra, two 4′-alkoxy-4-cyanobiphenyl model compounds (abbreviated as 10-OCB and 11-OCB) are studied:

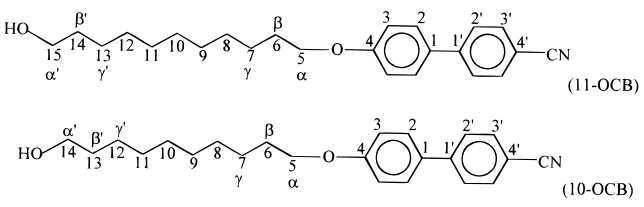

In comparison, the solution ^{13}C NMR spectra and the resonance assignments of 11-OCB and PEFBP(11) are shown in parts a and b of Figure 2 in $CDCl_3$, respectively. In Figure 2a, the ^{13}C chemical shifts of the side-chain CH_2 units are influenced by the substituent effects of the oxygen (O) atoms. For alkyl chains consisting of more than five carbons, the O atoms have a positive substituent effect (deshielding) on the α-carbons (C5/C15 at 68.3/63.2 ppm) and *β*-carbons (C6/C14 at 32.9/29.7 ppm). A negative substituent effect (shielding) can be observed on the *γ*-carbons (C7/C13 at 26.1/25.9 ppm).[24] The O atoms do not significantly affect the rest of the carbons due to the short-range nature of the chemical shift interaction. The signals from C8 to C12 overlap in a narrow region from 29.7 to 29.3 ppm. The chemical shifts for the aromatic carbon sites in the 4-cyanobiphenyls are assigned considering the substituent effects. Similar analyses were also been applied to the solution ^{13}C NMR spectra of 10-OCB and PEFBP(10) in DMSO-d_6. The chemical shifts for the model compounds (10-OCB and 11-OCB) and the aliphatic−mesogenic side chains in PEFBPs(*n*) (*n* = 10 and 11) are listed in Table 1 and are consistent with published data.[25,26]

Table 1. Chemical Shifts (ppm) of the Different Carbon Atoms in the LC Model Compounds and Aliphatic−Mesogenic Side Chains of PEFBPs(*n*) (*n* = 10 and 11) in Solution ^{13}C NMR

carbon	10-OCB[b]	PEFBP(10)[b]	carbon	11-OCB[a]	PEFBP(11)[a]
(C═O)s		167.0	(C═O)s		166.9
1	130.3	130.2	1	131.5	131.5
2	128.3	128.3	2	128.5	128.3
3	115.1	115.0	3	115.3	115.0
4	159.5	159.5	4	160.1	159.5
1′	144.3	144.3	1′	145.5	144.3
2′	126.8	126.8	2′	127.3	126.8
3′	132.8	132.8	3′	132.8	132.8
4′	109.1	110.2	4′	110.2	110.2
CN	119.0	119.2	CN	119.3	119.0
5	67.6	68.5	5	68.3	68.7
6	32.5	29.7	6	32.9	29.7
7	25.6	26.4	7	26.1	26.1
8−11	29.0−28.6	29.5−28.8	8−12	29.7−29.3	29.4−28.4
12	25.4	26.2	13	25.9	26.0
13	29.0	29.7	14	29.7	29.7
14	60.7	65.1	15	63.2	65.9

[a] $CDCl_3$. [b] DMSO-d_6.

Table 2. Chemical Shifts (ppm) of Different Carbon Atoms in the Backbones of PEFBPs(*n*) (*n* = 10 and 11) in Solution and Solid-State ^{13}C NMR

carbon	PEFBP(10)[b]	PEFBP(11)[a]	PEFBP(10)[c]	PEFBP(11)[c]
(C═O)s	167.0	166.9	166.0	166.6
(C═O)m	163.5	163.5	163.6	163.4
16	141.8	141.8	142.2	142.3
17	126.2	126.2		
18	120.7	120.7	121.0	121.9
19	131.9	131.9	131.7	131.9
20	132.1	132.1	132.0	132.1
21	131.6	131.6	131.5	131.9
22	140.2	140.2	140.8	141.0
23	130.4	130.4	130.5	130.1
24	123.4	123.4		
25	150.0	150.0	150.2	151.4
26	124.9	124.9		
27	129.5	129.5	129.1	129.5
$CF_{3(1:3:3:1)}$	126−124	126−124		

[a] $CDCl_3$. [b] DMSO-d_6. [c] Bloch decay spectrum in the isotropic melt.

The chemical shifts of the aromatic backbone carbons of PEFBPs(*n*) (*n* = 10 and 11) obtained from solution ^{13}C NMR and Bloch decay ^{13}C NMR in the I melt are provided in Table 2. The chemical structures of PEFBPs(*n*) (*n* = 10 and 11) and corresponding carbon number are labeled as follows:

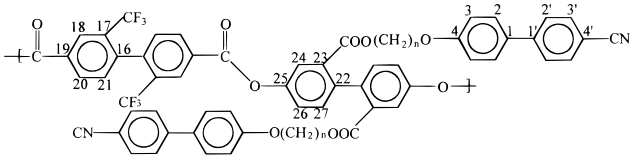

Note that 10-OCB and PEFBP(10) are dissolved in DMSO-d_6 while 11-OCB and PEFBP(11) are soluble in $CDCl_3$.

Variable-Temperature Solid-State ^{13}C NMR Spectra in PEFBP(10). As shown in Figure 3, both the ^{13}C CP/MAS and Bloch decay NMR spectra of PEFBP(10) are recorded upon heating. The detailed carbon sites in CP/MAS and Bloch decay at different temperatures are summarized in Table 3. The CP/MAS experiment conducted at 65 °C (above the T_g) provides information on the rigid component of the polymer exhibiting the intense resonance. The intense signals arise from the aromatic main chains at C25, C16/22, and C19−21 as well as the side chain carbons at C4, C4′, C3, C3′, and C1 (Table 3). A spinning sideband (SSB) at approximately 40 ppm is observed and the methylene carbon sites occur at 30.8 ppm. This reflects that the rigid components include the main chains, mesogens, and certain methylene units in the side chains. On the other hand, the side chains and the backbones can also be detected in the Bloch decay spectrum (Table 3), which is characteristic of low ordered LCPs.[18] The CP/MAS and Bloch decay spectra at 120 °C do not exhibit significant differences from those at 65 °C.

As the sample enters the N phase at 177 °C overall intensity of the CP/MAS spectrum is reduced with no SSB observation even though the signals of carbon sites in the 4-cyanobiphenyls and the backbones are detectable in this spectrum. This inefficient CP results from the weak and mobile C−H dipolar interactions, indicating that the population of rigid components has decreased significantly. The line-widths of the Bloch decay spectrum narrow and intensities are enhanced, reflecting that the system has achieved mobility. In the isotropization temperature region at 200 °C, only an intense Bloch decay spectrum with narrow line-widths is observed since the entire polymer is in the mobile liquid state (Table 3). The chemical shift for the methylene units at 29.8 ppm reveals that they possess rapid *trans-gauche* exchange conformations.[24]

Variable-Temperature Solid-State ^{13}C NMR Spectra in PEFBP(11). The ^{13}C CP/MAS NMR experiment of PEFBP(11) performed at 60 °C in the K_O crystal phase (T_g = 50 °C) exhibits intense resonance, as shown in Figure 4a. The detailed carbon sites for PEFBP(11) at different temperatures in the CP/MAS spectra are listed in Table 4. In addition to the carbonyl (C═O) nuclei at 166 ppm, the ^{13}C signals of the aromatic carbons in both the backbones (C25, C16/22, C19−21) and side chains (C4, C4′, C3, C3′, C2/2′, C1) are also intense. This reflects that the rigid components include both the backbones and the side-chain mesogens. The Bloch decay (Figure 4b) also detects the presence of both the side chains and backbones (Table 4). The resonance of the methylene units is observed at 31.0 ppm, indicating that the methylene units include the detectable gauche conformations. The CP/MAS (Figure 4a) and Block decay (Figure 4b) results at 90 °C are almost identical to those at 60 °C.

At 110 °C in the K_{T1} crystal phase, the CP/MAS spectrum in Figure 4a shows a change in intensity involving the backbones (C25, C16/22, and C19−21) and the side-chain mesogens (C4, C3, C3′, C2/2′, and C1). However, the C4′ signal is absent (Table 4), which may indicate a new chain conformation in the rigid component (in the K_{T1} phase). The chemical shift of the methylene units remains at 31.0 ppm, revealing the existence of gauche conformations in the aliphatic side chains. The Bloch decay spectrum (Figure 4b) shows that the C4, C4′, C3, C3′, C2/2′, and C1 in the side chains are distinguishable in the aromatic region, while the weak signal of the backbone C25 nuclei at 151 ppm disappears at this temperature (Table 4).

In the K_{T2} crystal phase at 130 °C, the CP/MAS (Figure 4a) exhibits substantial changes in line-widths and chemical shifts. Intense resonance for both the aromatic and aliphatic regions is observed in this spectrum (Table 4). The resonance of C5/15 splits into two individual signals at 69.5 ppm (C5) and 66.3 ppm

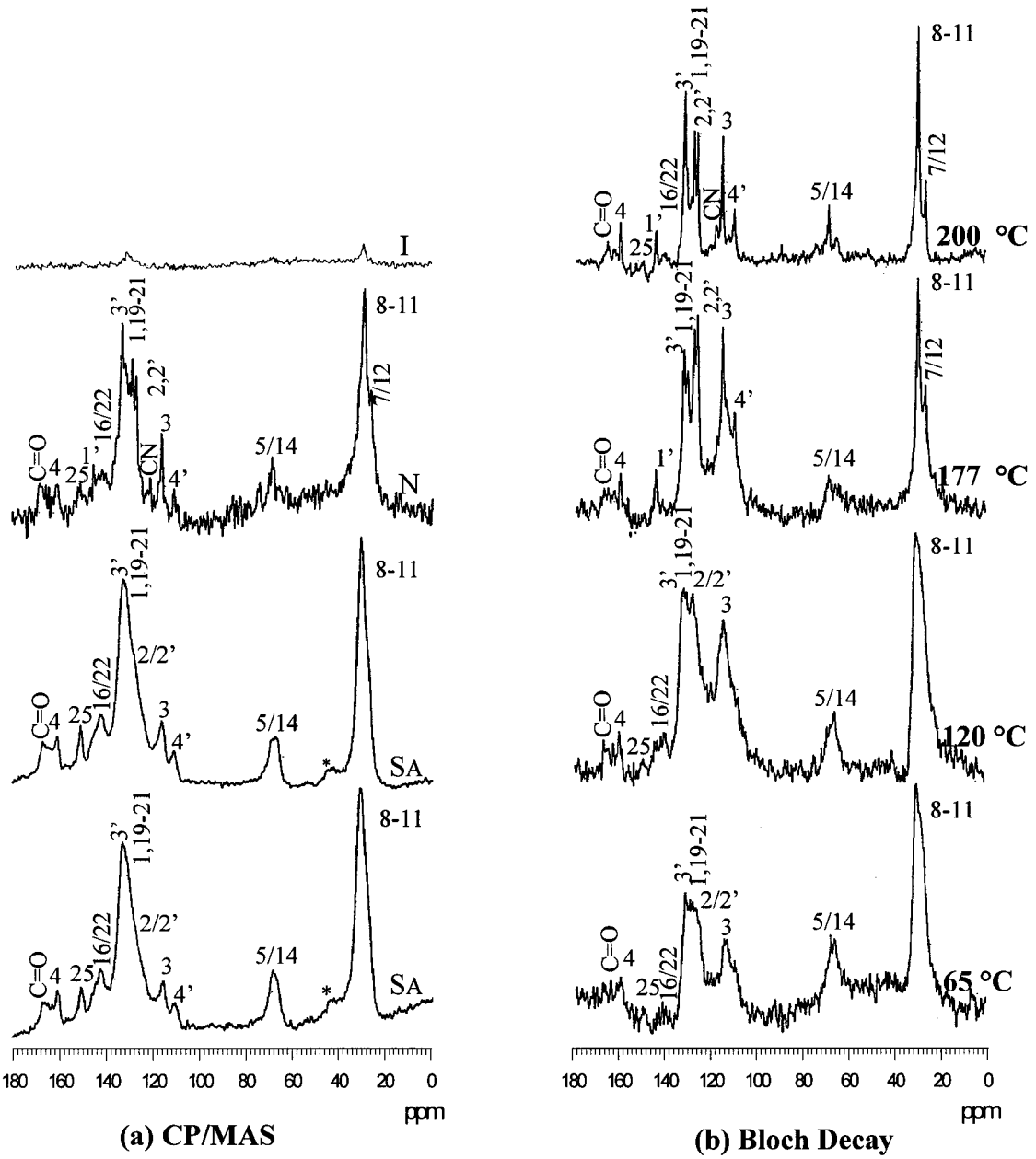

Figure 3. Solid-state ^{13}C NMR spectra of PEFBP(10) at various temperatures ranging from above the glass transition temperature to the isotropic melt: (a) CP/MAS spectra and (b) Bloch decay spectra. (note that ∗ stands for SSB).

Table 3. Variable-Temperature ^{13}C MNR Spectra for PEFBP(10)

temp, °C (phase)	backbone carbons		side chain carbons[a]
65 (smectic)	CP/MAS	25, 16/22, 19−21	8−11, 5/14, 4, 4′, 3, 3′, (2/2′),[b] 1
	Bloch	25, 16/22, 19−21	8−11, 5/14, 4, 3, 3′,2/2′, 1
120 (smectic)	CP/MAS	25, 16/22, 19−21	8−11, 5/14, 4, 4′, 3, 3,′, (2/2′)[b], 1
	Bloch	25, 16/22, 19−21	8−11, 5/14, 4, 3, 3′, 2/2′, 1
177 (nematic)	CP/MAS	25, 16/22, 19−21	8−11, 5/14, **7/12**, **CN**, 4, 4′, 3, 3′, 2, 2′, 1 **1′**
	Bloch	19−21	8−11, 5/14, **7/12**, 4,**4′**, 3, 3′, 2, 2′, 1 **1′**
200 (isotropic)	CP/MAS	-	-
	Bloch	25, 16/22, 19−21	8−11, 5/14, 7/12, **CN**, 4, 4′, 3, 3′, 2, 2′, 1, 1′

[a] The "/" represents overlapped chemical shifts; the bold number represents new chemical shifts occurring at elevated temperatures. [b] The signal in parentheses is very weak.

(C15). A substantial increase in the proportion of the rigid components is consistent with our WAXD results since the K_{T2} phase possesses a high crystallinity (over 70%).[11] The rigid components include the backbones (C25, C16/C22, C19−21) and the side-chain mesogens (C4, C4′, C3′, C3, C2, C2′, C1). The methylene units at 31.2 ppm indicate that the methylene sequence still contains gauche conformations, indicating that the methylene sequence is significantly different from the all-trans conformation at the position of 33−34 ppm.[18,20,21,27−29] The Bloch decay spectrum in the K_{T2} phase (Figure 4b) is also different from those of in the K_O and K_{T1} phases. The chemical resonance of the side-chain mesogens, aromatic backbones and methylene

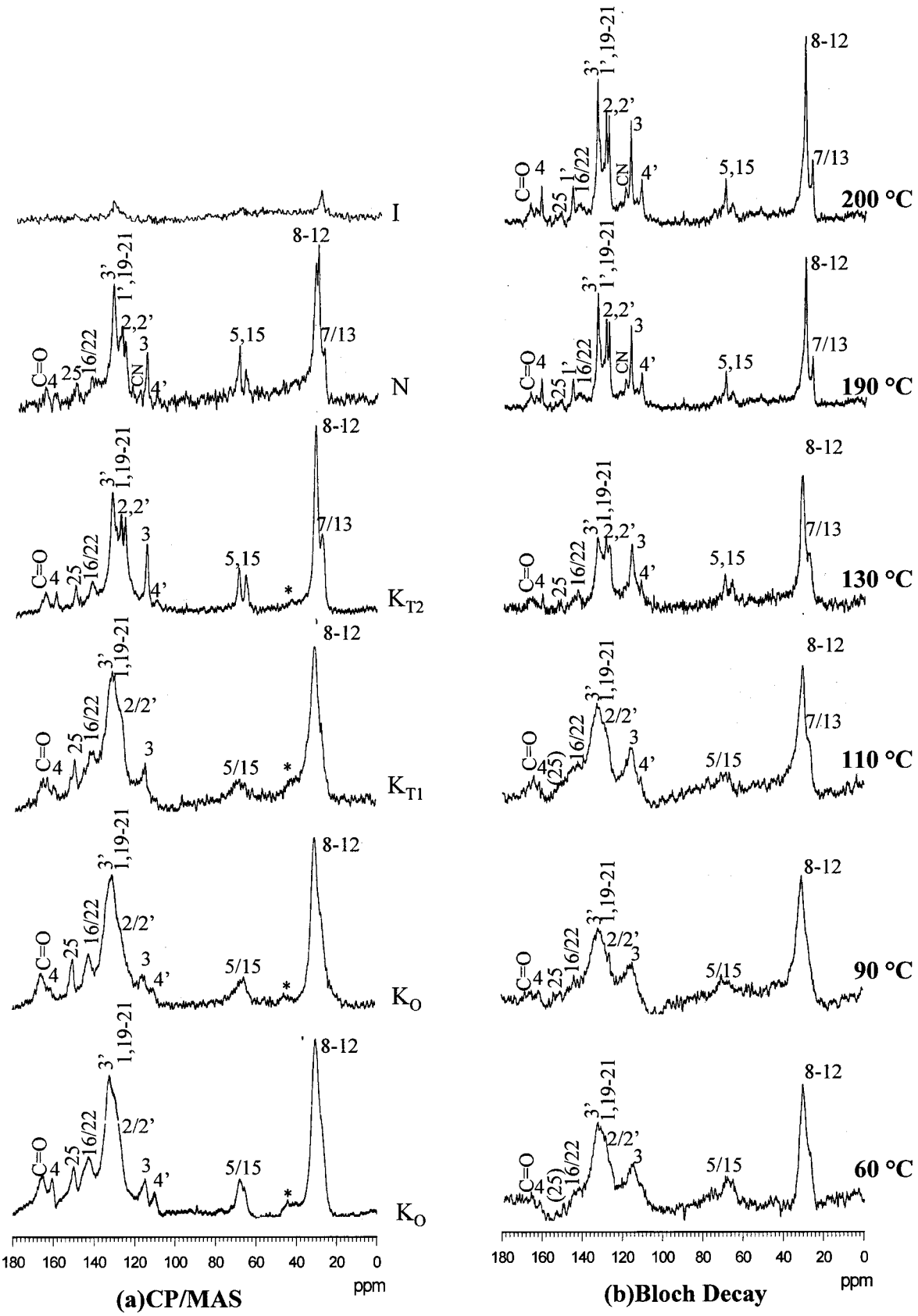

Figure 4. Solid-state ^{13}C NMR spectra of PEFBP(11) at various temperatures ranging from above the glass transition temperature to the isotropic melt: (a) CP/MAS spectra and (b) Bloch decay spectra (note that ∗ stands for SSB).

units are detectable (Table 4), but are reduced in intensity and the line-widths are narrowed.

When the N phase is entered at 190 °C, the intensity of the CP/MAS (Figure 4a) starts to decrease, while the intensity in the Bloch decay (Figure 4b) inverts. This indicates that the PEFBP(11) molecules become mobile, which is a characteristic of a N phase. The residual rigid components in the CP/MAS include the backbones and 4-cyanobiphenyl mesogens (Table 4), while the Bloch decay results (Figure 4b) show all the carbon sites of

Table 4. Variable-Temperature ^{13}C MNR Spectra for PEFBP(11)

temp, °C (phase)	backbone carbons		side chain carbons[a]
60 (Ko, crystal)	CP/MAS	25, 16/22, 19−21	8−12, 5/15, 4, 4′, 3, 3′, (2/2′)[b], 1
	Bloch	(25),[b] 16/22, 19−21	8−12, 5/15, 4, 3, 3′,2/2′, 1
90 (Ko, crystal)	CP/MAS	25, 16/22, 19−21	8−12, 5/15, 4, 4′, 3, 3′, (2/2′)[b], 1
	Bloch	25, 16/22, 19−21	8−12, 5/15, 4, 3, 3′, 2/2′, 1
110 (K_{T1}, crystal)	CP/MAS	25, 16/22, 19−21	8−12, 5/15, 4, 3, 3′, 2/2′, 1
	Bloch	16/22, 19−21	8−12, 5/15, **7/13**, 4, **4′**, 3, 3′, 2, 2′, 1
130 (K_{T2}, crystal)	CP/MAS	25, 16/22, 19−21	8−12, **5 15**, **7/13**, 4, **4′**, 3, 3′, 2, 2′, 1
	Bloch	25, 16/22, 19−21	8−12, **5 15**, 7/13, 4, 4′, 3, 3′, 2, 2′, 1
190 (nematic)	CP/MAS	25, 16/22, 19−21	8−12, 5, 15, 7/13, **CN**, 4, **4′**, 3, 3′, 2, 2′, 1
	Bloch	25, 16/22, 19−21	8−12, **5 15**, 7/13, **CN**, 4, 4′, 3, 3′, **2, 2′**, 1 **1′**
200 (isotropic)	CP/MAS	-	-
	Bloch	25, 16/22, 19−21	8−12, 5, 15, 7/13, CN, 4, 4′, 3, 3′, 2, 2′, 1, 1′

[a] The "/" represents overlapped chemical shifts; the bold number represents new chemical shifts occurring at elevated temperatures. [b] The signal in parentheses is very weak.

the backbones and side chains. Above the isotropization temperature at 200 °C, an intense Bloch decay spectrum is observed (Figure 4b, Table 4), revealing that the mobile components dominate the system. The resonance of the methylene units shifts toward 29.8 ppm.

The experimental results indicate that the effect of the odd−even methylene units on the phase transitions of PEFBPs does not simply originate in a change from trans to gauche conformations in the methylene units. An all-trans conformation sequence is not detected over the temperature range studied in either of PEFBPs(n) (n = 10 or 11). Detectable portions of the methylene units in the side chains possess gauche conformations in the ordered crystalline phases of PEFBP(11). This characteristic feature differs from that of main-chain LCPs[18,20,22] and hairy-rod polymers[17,21] with their board-like structures. The gauche conformations provide a folded array for the methylene units, leading to dense parallel packing of the side-chain mesogens with the backbones in the crystals for PEFBP(11). This is in agreement with our explanation of the cocrystallized packing model of the side-chain mesogens parallel to the backbones.[11,13] The same principle also holds for the construction of LC phases in PEFBPs(n) (n = 10 and 11). If the side chains aggregate and crystallize independently from the backbones, the backbones and side-chain mesogens can generate two separate domains.

CP/MAS Proton Spin−Spin and Spin−Lattice Relaxation Behavior. To further investigate the possible heterogeneity due to the microphase separation in these systems, we have employed high-power proton decoupling with MAS, which is typical for solid-state ^{13}C NMR analysis to distinguish between ordered crystalline and disordered amorphous regions.[19,30−32] The main purpose of the experiments is to determine whether there is a difference between relaxation times corresponding to the side chains from the backbones. CP/MAS proton spin−spin and spin−lattice relaxation times are used to characterize relaxation processes of $^{H}T_2$ and $^{H}T_{1\rho}$.

For the determination of $^{H}T_2$, the intensities of the resonance for different carbon sites uniformly decrease as a function of the pulse delay, ranging from 1 to 60 μs. Figure 5a shows a stacked set of ^{13}C NMR spectra of the proton spin−spin relaxation for PEFBP(11) in the K_{T2} phase at 80 °C. The extremely weak intensity of the resonance in PEFBP(11) at 60 μs indicates that it is almost completely dephased. The corresponding intensity decays as a function of delay time for PEFBP(11) are plotted in Figure 5b for selected carbon sites. It is observed that the changes in the intensity vs delay times can be fitted into a single-exponential decay function of $I = A \exp\{-(\tau/^{H}T_2)^2\}$. The NMR results for PEFBP(11) in the K_{T2} phase at 80 °C lead to $^{H}T_2$ values of 22.7 μs (the aromatic carbons at 132.0 ppm), 23.8 μs (the side-chain mesogenic carbons at 115.5 ppm), and 22.6 μs (the methylene carbons at 31.2 ppm). The $^{H}T_2$ relaxation times of the different carbon sites are surprisingly comparable, indicating homogeneous dynamics throughout. Similarly, $^{H}T_2$ values can be obtained in the S_A phase of PEFBP(10) and in the other crystal phases of PEFBP(11). For example, PEFBP(10) in the S_A phase at 80 °C has identical and $^{H}T_2$ values of 38 ± 2 μs for the different carbon sites in the side chains and the backbones. The hairy-rod polymers without pendent mesogens in the methylene side chains possess two different $^{H}T_2$ relaxation times at 70 °C: (1) 50 μs, corresponding to the methylene units in the side chains, and (2) 30 μs, corresponding to the aromatic backbones.[23] Microphase segregation between the molten side chains and the rigid backbones presumably occurs. The observed identical $^{H}T_2$ values for the backbones, side-chain mesogens, and methylene units in these two PEFBPs are unique characteristics of this system.

The spin diffusion coefficient (D) can be calculated directly from the spin−spin relaxation measurements.[33,34] The equation used is $D = 2r_o^2/^{H}T_2$, where r_o is the proton van der Waals radius of 0.117 nm. The calculated D for the different carbon sites of PEFBP(11) in the K_{T2} phase at 80 °C is 1.19 nm^2/ms using $^{H}T_2 = 23$ μs. Similarly, D = 0.72 nm^2/ms for PEFBP(10) in the S_A phase at 80 °C (the spin diffusion coefficients may also be calculated from the transverse relaxation rate T_2^{-1} [35,36]). The domain sizes can be correlated with the molecular dynamics in each phase of PEFBPs(n) (n = 10 and 11) based on the calculated coefficients.

In general, molecular motions in different ordered regions above the T_g can also be distinguished by the spin−lattice relaxation time $^{H}T_{1\rho}$ in the rotating frame. Figure 6a shows a stacked set of ^{13}C NMR spectra of the proton spin−lattice relaxation in the rotating frame for PEFBP(10) in the S_A phase at 80 °C. These spectra are recorded as a function of the proton spin lock time prior to the CP from 0.01 to 40 ms. The corresponding intensity decays as a function of the time for PEFBP(10) are plotted at selected carbon sites, as shown in Figure 6b. Only a single-exponential decay function of $I = A \exp(-\tau/^{H}T_{1\rho})$ is required to fit the experimental data. The $^{H}T_{1\rho}$ values in the S_A phase of PEFBP(10) at 80 °C are 8.2 ms (the methylene C8−11 side chains at 30.8 ppm), 7.8 ms (the aromatic carbons in both the backbones and the side chains of C3′, C1, and C19−21 at

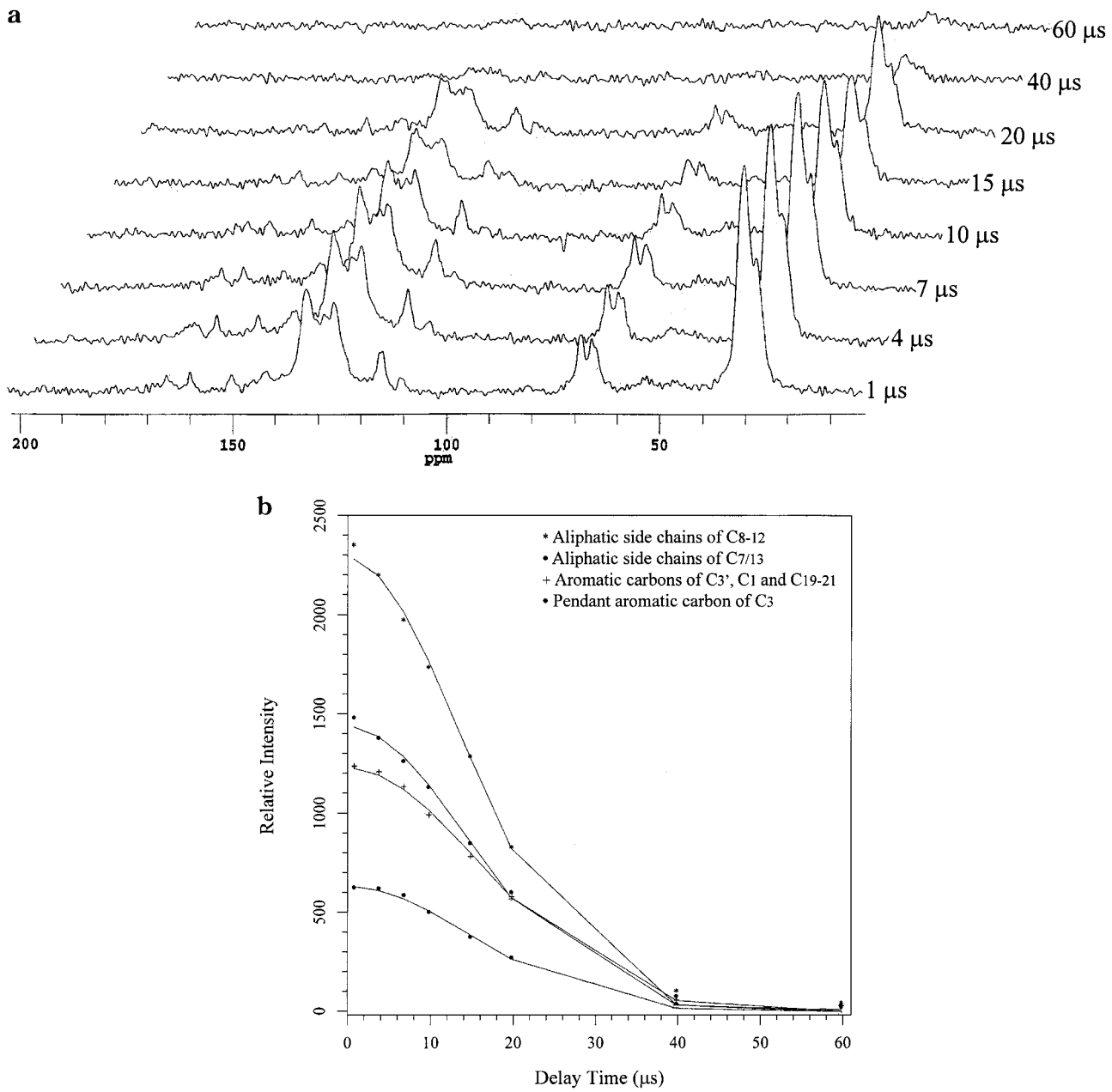

Figure 5. Solid-state ^{13}C NMR stacked spectra of the proton spin−spin relaxation ($^{H}T_2$) for PEFBP(11) in the K_{T2} phase at 80 °C at different delay times (a). ^{13}C NMR intensity change vs delay time of PEFBP(11) for the K_{T2} phase at 80 °C (b).

132.0 ppm), and 7.8 ms (the C_3 pendant mesogenic carbon at 115.5 ppm). These identical $^{H}T_{1\rho}$ values indicate that the system is homogeneous.

The ^{13}C intensities and spin lock times measured in the K_{T2} phase at 80 °C are shown in Figure 7 (from 0.01 to 40 ms) for PEFBP(11) after the sample was isothermally crystallized at 130 °C. The $^{H}T_{1\rho}$ values calculated are also identical for the different carbon sites (19.4 ± 1 ms), and exhibit a single component relaxation process. Single-exponential relaxation processes can also be used for the other crystalline phases in PEFBP(11), although the absolute values of $^{H}T_{1\rho}$ varies within each phase.

It is surprising that the $^{H}T_{1\rho}$ data in each of the crystalline and LC phases of PEFBPs(n) (n = 10 and 11) show identical values among the different carbon sites. Both the side chains and the backbones in these phases share the same homogeneous dynamics with respect to molecular motions. The remaining question concerns the homogeneous domain size of these phases. The proton spin diffusion experiments can be used to estimate the domain sizes of heterogeneous (microphase-separated) systems. The domain size is calculated semiquantitatively from the one-dimensional diffusion equation[30,31,33,34] of $\langle r^2 \rangle = (4/3)D\tau_e$, where $\langle r \rangle$ is the diffusion distance, τ_e is the spin diffusion time, and D is the spin diffusion coefficient obtained based on $^{H}T_2$. Setting $^{H}T_{1\rho}$ (or $^{H}T_1$) equal to time τ_e, domain sizes ranging from 1 to 100 nm are calculated.[37−39] On the time scale of $^{H}T_{1\rho}$ (τ_e = 8 ms) in the S_A phase of PEFBP(10), no microphase segregated domains should be observed on a size scale exceeding 3 nm. The identical $^{H}T_{1\rho}$ values imply that the ^{1}H spins in the different domains are fully exchanged on this time scale, indicating that the system is homogeneous as the domain size exceeds 3 nm.

In the case of the K_{T2} phase of PEFBP(11), the substantial increase in the $^{H}T_{1\rho}$ relaxation time is due

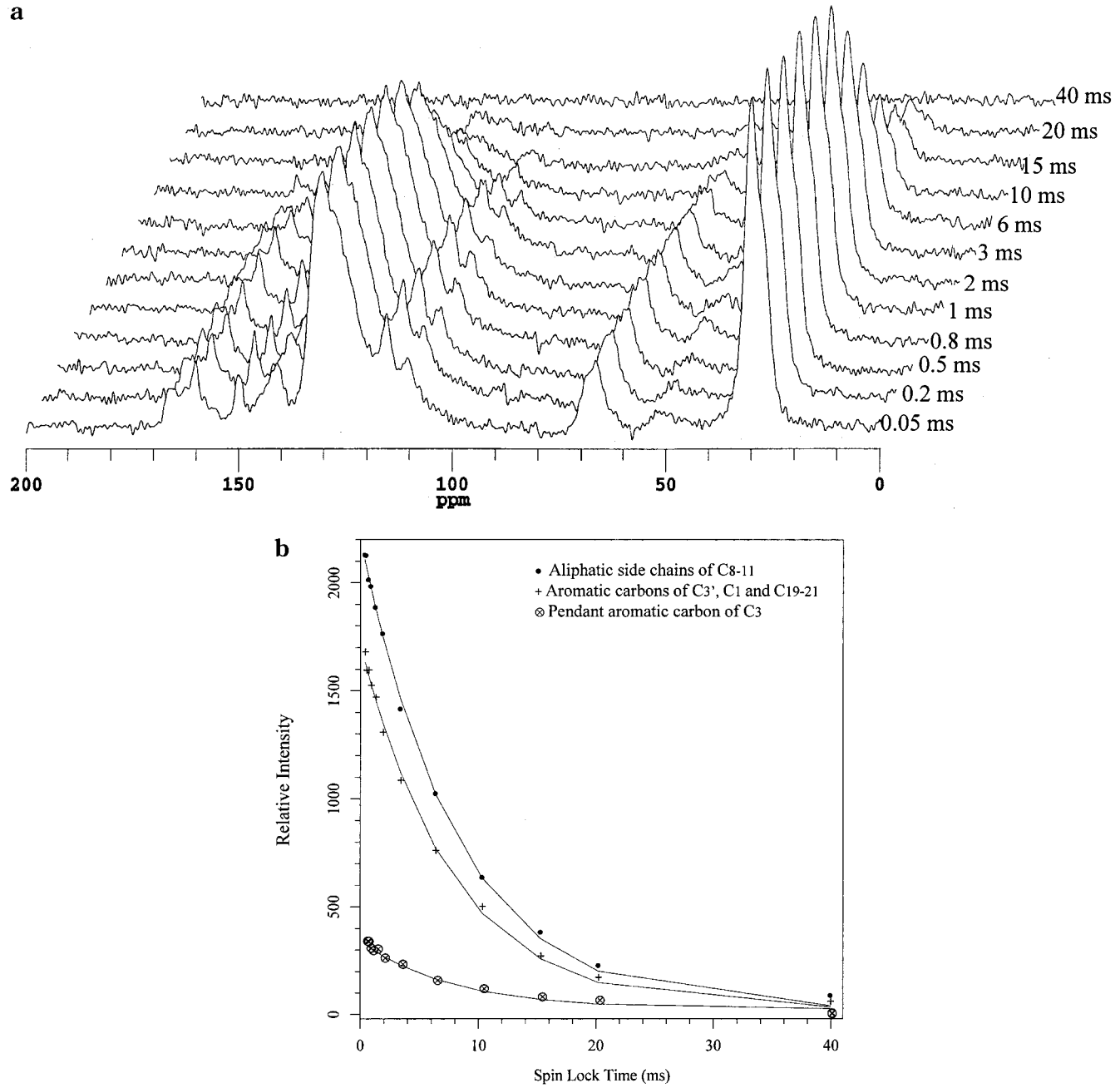

Figure 6. Solid-state ^{13}C NMR stacked spectra of the proton spin−lattice relaxation ($^{H}T_{1\rho}$) in the rotating frame for PEFBP(10) in the S_A phase at 80 °C at different spin lock times (a). ^{13}C NMR intensity change vs spin lock time of PEFBP(10) for the S_A phase at 80 °C (b).

to the restricted motion of this highly ordered crystalline phase.[19] The $^{H}T_{1\rho}$ values for the different carbon sites are also identical. On the basis of the diffusion equation, an individual domain size of 6 nm can be calculated using $\tau_e = 19.4$ ms obtained from the $^{H}T_{1\rho}$ experiments. Homogeneous dynamics thus takes place on a size scale greater than 6 nm, indicating that both the backbones and side chains are incorporated into one crystal lattice. Note that the K_{T2} phase is 70% crystalline and therefore, 30% of the material is in the N phase. It is speculated that the N phase must be existed in a domain size of less than 6 nm.

Conclusion

In PEFBP(10), ^{13}C CP/MAS NMR analyses indicate that both the backbones and side-chain mesogens are involved in the formation of the S_A and N phases. In PEFBP(11), sets of CP/MAS spectra in the K_O, K_{T1}, and K_{T2} phases show that the methylene units in the side chains possess gauche conformations. These gauche conformations are necessary to adopt a folded array for the side-chain mesogens to align parallel to the backbones and fit in a three-dimensional crystalline lattice. In addition, the formation of the N phase in PEFBP(11) is also attributed to a cooperative effort of the mesogens in both the side chains and the backbones. The $^{H}T_{1\rho}$ and $^{H}T_2$ analyses demonstrate that both the side chains and backbones possess single-exponential relaxation processes in the crystalline phases of PEFBP(11) and the homogeneous domains are observed on a size scale exceeding 6 nm. However, the homogeneous dynamics in the S_A phase of PEFBP(10) occur on a size scale exceeding 3 nm. Further work is required to correlate

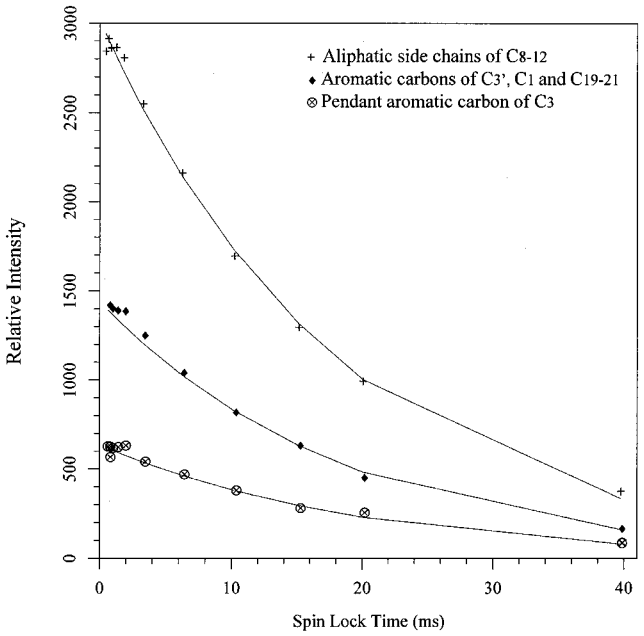

Figure 7. Solid-state ^{13}C NMR intensity change vs spin lock time in $^{H}T_{1\rho}$ experiments of PEFBP(11) for the K_{T2} phase at 80 °C.

the dynamic relaxation behavior with the structural analyses.

Acknowledgment. This work was supported by the National Science Foundation (DMR-96-17030) and the Science and Technology Center for Advanced Liquid Crystal Optical Materials (ALCOM) at Kent State University, Case Western Reserve University, and University of Akron.

References and Notes

(1) Seki, T.; Sakuragi, M.; Kawanishi, Y.; Suzuki, Y.; Tamaki, T.; Fukuda, R.; Ichimura, K. *Langmuir* **1993**, *9*, 211.
(2) Kang, C. S.; Winklehahn, H. J.; Schulz, M.; Neher, D.; Wegner, G. *Chem. Mater.* **1994**, *6*, 2159.
(3) Ge, J. J.; Xue, G.; Li, F.; Wang, S.-Y.; Harris, F. W.; Cheng, S. Z. D.; Zhuang, X.; Hong, S.-C.; Shen, Y. R *Macromol. Rapid Commun.* **1998**, *19*, 619.
(4) Gray, G. W. *Advances in Liquid Crystals for Material Applications*. BDH Chem.: Poole, England, 1978.
(5) Reck, B.; Ringsdorf, H. *Macromol. Rapid Commun.* **1985**, *6*, 291.
(6) Reck, B.; Ringsdorf, H. *Macromol. Rapid Commun.* **1986**, *7*, 389.
(7) Zental, R.; Recket, G.; Reck, B. *Liq. Cryst.* **1987**, *2*, 83.
(8) Endres, B. W.; Ebert, M.; Webdorff, J. H.; Reck, B.; Ringsdorf, H. *Liq. Cryst.* **1990**, *7*, 217.
(9) Kappitza, Z.; Zental, R. *Macromol. Chem.* **1991**, *192*, 1859.
(10) Wang, S.-Y. Ph.D. Dissertation, Department of Polymer Science, The University of Akron, Akron, OH 44325-3909, 1995.
(11) Ge, J. J.; Zhang, A.; McCreight, K. W.; Ho, R.-M.; Wang, S.-Y.; Jin, X.; Harris, F. W.; Cheng, S. Z. D. *Macromolecules* **1997**, *30*, 6498.
(12) Ge, J. J.; Zhang, A.; McCreight, K. W.; Wang, S.-Y.; Harris, F. W.; Cheng, S. Z. D. *Macromolecules* **1998**, *31*, 4093.
(13) Ge, J. J.; Honigfort, P. S.; Ho, R.-M.; Wang, S.-Y.; Harris, F. W.; Cheng, S. Z. D. *Macromol. Chem. Phys.* **1999**, *200*, 31.
(14) Herrmann-Schonherr, O.; Wendorff, J. H.; Ringsdorf, H.; Tschirner, P. *Macromol. Rapid Commun.* **1986**, *7*, 791.
(15) Ballauff, M.; Schmidt, G. F. *Macromol. Rapid Commun.* **1987**, *8*, 93.
(16) Adam, A.; Spiess, W. *Macromol. Rapid Commun.* **1990**, *11*, 249.
(17) Kricheldorf, H. R.; Domschke, A. *Macromolecules* **1996**, *29*, 1337.
(18) Cheng, J.; Jin, Y.; Wunderlich, B.; Cheng, S. Z. D.; Yandrasits, M. A.; Zhang, A.; Pecec, V. *Macromolecules* **1992**, *25*, 5991.
(19) Perez, E.; Marugan, M. M.; VanderHart, *Macromolecules* **1993**, *26*, 5852.
(20) Cheng, J.; Jin, Y.; Wunderlich, B.; Jonsson, H.; Hult, A.; Gedde, U. W. *J. Polym. Sci., Part B: Polym. Phys.* **1994**, *32*, 721.
(21) Sone, M.; Harkness, B. R.; Kurosu, H.; Ando, I.; Watanabe, J. *Macromolecules* **1994**, *27*, 2769.
(22) Cheng, J.; Yoon, Y.; Ho, R.; Leland, M.; Guo, M. M.; Cheng, S. Z. D.; Chu, P.; Pecec, V. *Macromolecules* **1997**, *30*, 4688.
(23) McCreight, K. W.; Ge, J. J.; Guo, M.; Mann, I. K.; Li, F.; Shen, Z.; Jin, X.; Harris, F. W.; Cheng, S. Z. D. *J. Polym. Sci., Part B: Polym. Phys.* **1999**, *37*, 1633.
(24) Tonelli, A. E. *NMR Spectroscopy and Polymer Microstructure, The Conformational Connection*; VCH Publishers: New York, 1989.
(25) Hvilsted, S.; Andruzzi, F.; Kulinna, C.; Siester, H.; Ramanujam, P. S. *Macromolecules* **1995**, *28*, 2172.
(26) Neol, C.; Gangadhara; Ching, K. C.; Large, M.; Reyx, D.; Kajzar, F. *Macromol. Chem. Phys.* **1997**, *198*, 1665.
(27) Kuwabara, K.; Horii, F. *Macromolecules* **1999**, *32*, 5600.
(28) VanderHart, D. L. *J. Chem. Phys.* **1986**, *84*, 1196.
(29) Ishida, M.; Kaji, H.; Horii, F. *Macromolecules* **1997**, *30*, 5799.
(30) Havens, J. R.; VanderHart, D. L. *Macromolecules* **1985**, *18*, 1663.
(31) Ishida, M.; Yoshinaga, K.; Horii, F. *Macromolecules* **1996**, *29*, 8824.
(32) Guo, M. M. *Trends in Polymer Science* **1996**, *4*, 238.
(33) VanderHart, D. L. *Macromol. Chem. Macromol. Symp.* **1990**, *34*, 125.
(34) Egawa, Y.; Imanishi, J.; Matsumoto, A.; Horii, F. *Polymer* **1996**, *37*, 5569.
(35) Nagapudi, K.; Leison, J.; Bechham, H. W.; Gibson, H. W. *Macromolecules* **1999**, *32*, 5799.
(36) Mellinger, F.; Wilhelm, M.; Spiess, H. W. *Macromolecules* **1999**, *32*, 4686.
(37) Landfester, K.; Boeffel, C.; Lambla, M.; Speiss, H. W. *Macromolecules* **1996**, *29*, 5972.
(38) Spiegel, S.; Landerfester, K.; Leison, G.; Boeffel, C.; Speiss, H. W.; Eidam, N. *Macromol. Chem. Phys.* **1995**, *196*, 985.
(39) McBrierty, V. J.; Packer, K. J. *Nuclear Magnetic Resonance in Solid Polymers*; Cambridge University Press: New York, 1993.

MA981970Y